Environmental Science Processes & Impacts

Radium in hydraulic fracturing wastewater: Distribution in suspended solids and implications to its treatment by sulfate co-precipitation

Journal:	*Environmental Science: Processes & Impacts*
Manuscript ID	EM-ART-07-2018-000311.R2
Article Type:	Paper
Date Submitted by the Author:	23-Nov-2018
Complete List of Authors:	Ouyang, Bingjie; Dartmouth College, Earth Sciences Renock, Devon; Dartmouth College, Earth Sciences Ajemigbitse, Moses; Penn State, Van Sice, Katherine; Penn State Warner, Nathaniel; Penn State, CEE; Penn State CEE Landis, Joshua; Dartmouth College, Earth Sciences Feng, Xiahong; Dartmouth College, Earth Sciences

With the application of hydraulic fracturing during oil & gas extraction, high volumes of wastewater generated in this process brought along a variety of anthropogenic and natural contaminants. Among the contaminants, radium, with activities up to 10,000 pCi/L, is the dominant technologically enhanced naturally occurring radioactive material. The distribution of radium in solid waste, radium mobility in natural environment, as well as its effective treatment have been emerging concerns. This work discovered that more than half of the radium in fresh wastewater solids were labile and suggested these solids should be treated prior to disposal. By assessing the radium treatment method of sulfate co-precipitation, this work provides insights to optimal radium treatment conditions.

Radium in hydraulic fracturing wastewater: Distribution in suspended solids and implications to its treatment by sulfate co-precipitation

Authors: Bingjie Ouyang,*† Devon J. Renock,† Moses A. Ajemigbitse,‡ Katherine Van Sice,‡ Nathaniel R. Warner,‡ Joshua D. Landis,† Xiahong Feng†

† Department of Earth Sciences, Dartmouth College, HB6105 Fairchild Hall, Hanover, New Hampshire 03755, United States

‡ Department of Civil and Environmental Engineering, Pennsylvania State University, 212 Sackett Building, University Park, Pennsylvania 16802, United States

ABSTRACT

High concentrations of barium (Ba), strontium (Sr) and radium (Ra) are present in both the liquid and suspended solid portions of wastewater produced from hydraulic fracturing. These high concentrations often require special treatment in which the solid and liquid portions are separated and then independently treated prior to disposal. The solids are typically disposed in landfills while the liquids are further treated, recycled for future hydraulic fracturing, or disposed via injection wells. Finding optimal treatment methods of both the solid and the liquid fractions requires a thorough understanding of potential Ra mobility from both the raw suspended solids and mineral precipitates during treatment. Using a sequential extraction procedure, we found that, without treatment, more than 50% of Ra-226 in the suspended solids was associated with soluble salts and readily exchangeable fractions. When the liquid portion of the wastewater was treated by mixing with acid mine drainage (AMD), which contained high sulfate concentrations, approximately 80 - 97% of the total Ra-226 in the mixture solution is found in the insoluble sulfate fraction of the precipitate. The activity of Ra-226 sequestered in the precipitated solid sulfate fractions is positively correlated with the Sr/Ba ratio of the wastewater-AMD

* Corresponding Author:
Telephone: +1-603-306-9652.
E-mail: bingjie.ouyang.gr@dartmouth.edu

solution. We discuss implications of these findings for effective long-term management of elevated radium in both solid and liquid wastes.

1. INTRODUCTION

Large volumes of hypersaline wastewater with suspended solids return to the wellhead following high volume hydraulic fracturing (HVHF) [1–6]. The fluids that return to the surface within a few days are often termed as flowback water; the fluids return later (months to years) and persist for the entire duration of the well life are referred to as produced water[5,7,8]. In the Appalachian Basin, the wastewater is briny (with total dissolved solids [TDS] > 35,000 ppm); contains major cations (Na^+, Ca^{2+}, Ba^{2+}, and Sr^{2+}) with concentrations up to 100,000 ppm; and a major anion (Cl^-) up to 200,000 ppm [9–13]. Both the liquid and solid portions in the wastewater contain high levels of naturally occurring radioactive material (NORM); in particular, radium-226 (Ra-226) activity can be as high as 370 Bq/L (~10,000 pCi/L) in the liquids and 10 Bq/g (~270 pCi/g) in the untreated suspended solids [9–11,14–16]. Due to the high radioactivity in both liquid and solid portions, proper disposal of the HVHF waste is required, which remains a major concern and challenge to the field of waste management [9,12,17–19].

Important processes that may constrain the fate of Ra during hydraulic fracturing include co-precipitation, sorption, alpha recoil, and decay [20–25]. Among various Ra isotopes, Ra-223 and Ra-224 are less considered in the research of Ra transport due to their short half-lives (3.6 and 11.4 days respectively); Ra-228 has a relatively long half-life of 5.8 years but decays quickly within years; the 1602-year-long half-life of Ra-226 makes it an ideal isotope to study when not considering decay processes [26,27]. Alpha recoil happens

when the newly created daughter radionuclide recoils in the opposite direction of the ejected particle with energy 10^4-10^6 times greater than typical chemical bond energies, consequently, Ra may be liberated rapidly [28,29]. However, the chances of recoil process is generally small [30] and alpha recoil is reported to mostly affect the presence of Ra-224 [22]. Iron oxides, organic materials and clay minerals are shown to have great capacity to adsorb heavy metals and radionuclides [20,21,31], however, the extent of sorption to solid surfaces is reported to significantly decreased in the presence of saline produced fluids [32]. Due to their similar chemical properties, the fates of Ba, Sr and Ra during oil & gas production and waste disposal are often studied together [8,9,24,33–35]. Indeed, Ra, Ba and Sr often co-precipitate to form radio-barite/celestite in the presence of SO_4^{2-}, and Ra is thus removed from the liquid portion of the wastewater [18,24,36–38]. Therefore, among the key processes constraining Ra-226 transport, influences from processes like alpha recoil and decay are likely negligible compared to sorption and co-precipitation. Characterization of Ra-226 association with different mineral fractions in solid waste is important in understanding the processes that dominate Ra-226 distribution.

Previous studies have characterized Ra associated with three types of HVHF wastes: 1) shale cuttings, 2) raw liquid wastes and 3) waste sludge precipitated in waste impoundments. In Marcellus Shale cuttings, Landis *et al*. (2018) found that up to 14% of Ra was loosely-bound with operationally defined soluble salts, oxides, carbonates and organic compounds, susceptible to release under environmental conditions; whereas Ra bound to silicates and sulfates was more resistant to leaching and therefore remained immobilized [39]. Nelson *et al*. (2016) analyzed Marcellus produced water and presented strong partitioning of common NORMs among different mineral fractions and that the

partitioning is strongly correlated to ionic strength. However, Ra distribution in individual fractions was not the focus of this work [32]. Zhang *et al*. (2015) sought to identify mineral fractions containing Ra-226 using sequential extractions on waste sludge collected from centralized wastewater impoundments. The work by Zhang *et al*. (2015) was conducted in a systematic and rigorous manner focusing on waste sludge that had been stored in impoundments for up to two years prior to collection. During this period, the speciation of Ra-226 in the aged waste sludge is hypothesized to have changed significantly from the fresh suspended solid as it returned to the surface [33]. The changes may include oxidation of iron oxides and sulfides, precipitation of barite and celestite due to oversaturation or mixing with incompatible fluids, and enhanced sorption of Ra-226 onto oxides and clays due to extended reaction time. The suspended solids present in produced water shortly after it returns to the surface has not yet been characterized for Ra-226 distribution. In the liquid portion of the HVHF wastewater, Ra activity is often shown to correlate with high concentrations of Ba, Sr, total dissolved solids (TDS) [9, 11, 12, 23, 24] and Ca concentrations [20], suggesting that co-precipitation with these cations is likely an effective way to Ra removal.

In Ba/Sr/Ra-SO_4 co-precipitation, sufficient sulfate supply is often the limiting factor preventing removal of Ra in HVHF wastewaters; thus, addition of sulfate is an important treatment step [9,11]. Because AMD is rich in sulfate and often located nearby oil & gas wells, the mixture of acid mine drainage (AMD) and wastewater has been studied to evaluate Ba/Sr/Ra-SO_4 co-precipitation [8,40]. Kondash *et al*. (2014) demonstrated that mixing different proportions of AMD and wastewater resulted in 60% to 100% Ra removal [8]. He *et al*. (2016) further adjusted the mixing ratio of AMD and wastewater, and achieved greater than 99% Ra removal [40]. However, the effects of solution chemistry on Ra removal

and the composition of the co-precipitation solids have not been characterized to determine the optimal treatment conditions of AMD-HVHF wastewater mixture. For example, in Ra-SO_4 co-precipitation experiments (without using AMD or HVHF), the ionic strength of the solution and the presence of competing ions (e.g., Sr and Ca) were found to influence Ra removal efficiency [25,38]. Additionally, low Sr/Ba ratios favored Ra incorporation into radiobarite [24,41]. Likewise, these factors remain to be investigated with refined sequential extraction experiments in order to understand their influences on effectiveness of Ra sequestration in solids co-precipitated via mixture of AMD and HVHF wastewater.

The objectives of this study are: 1) To characterize the fresh suspended solids portion of HVHF wastewater (raw waste solid) using a comprehensive operationally-defined sequential extraction protocol [34]. We aim to quantify Ra activity extracted from different mineral fractions and compare the distribution of Ra with previous studies. 2) To characterize the solids formed during co-treatment of HVHF wastewater and AMD (waste treatment solid) using the same sequential extraction procedure. Specifically, we examine how different mixtures of AMD and HVHF wastewater, with varying solution chemistry, influence Ra re-distribution. We hypothesize that different solution chemistry will affect Ra incorporation into recalcitrant minerals. This work could ultimately provide guidance for disposal of wastes generated during HVHF.

2. MATERIALS AND METHODS

2.1 Materials

This study examined two solid materials generated during HVHF and its wastewater treatment - raw waste solid (RWS) and waste treatment solid (WTS). We

obtained a fresh produced water sample from a waste treatment facility in Pennsylvania and separated the liquid and solid portions by centrifugation at 4500 rpm (with a relative centrifugal force of 7000 g) for 1 hour. The liquid was decanted and the remaining solid was freeze-dried to obtain a RWS. The mineralogy of the RWS was analyzed by X-ray diffraction (XRD). The major cations of the liquid portion of the wastewater following separation were characterized with inductively coupled plasma optical emission spectrometry (ICP-OES). Both the mineralogy and water chemistry are presented in the Supplementary Information.

The waste treatment solids (WTS) were the solids precipitated after mixing two different HVHF wastewaters with three AMD samples. The Pennsylvania Department of Environmental Protection Bureau of Abandoned Mine Reclamation provided the AMD samples. Six samples of WTS were produced by mixing the unfiltered liquid portion of flowback water collected from two different Marcellus wells with three discharges of AMD in different proportions. Afterwards, the liquids were decanted, the WTS was harvested and freeze-dried [8]. All AMD and Marcellus flowback water were collected from Southwestern Pennsylvania. These AMD and flowback water sources were selected because they are from the same region; if the co-treatment is applied on a large scale, reducing transportation costs is economically and environmentally beneficial. The chemistry of HVHF wastewater in this study lies within the interquartile range of the produced water database for Marcellus wells reported by the USGS [42]. The AMD samples were representative of several large-volume discharges in Southwestern PA. The major ion concentrations for each AMD (I- II, and III) and flowback water (Flowback I and Flowback II) before mixing are given in Table S2 in the Supplementary Information. The major

minerals in the WTS detected by XRD included halite, barite, celestite, and marcasite (see detailed XRD results in Supplementary Information).

2.2 Sequential extraction

An operationally-defined sequential extraction procedure was used to quantify Ba, Sr and Ra in different mineral fractions in the RWS and WTS. This procedure has previously been demonstrated to quantitatively extract both Ba [34] and Ra [39,43] from Marcellus Shale. The sequential extraction involved digesting 2 g aliquots of each sample in a 50 mL polypropylene centrifuge tube by eight sequential steps:

(1) 12 mL deionized water (DI) (18 MΩ) was used to dissolve soluble salts.

(2) 12 mL 1 M $CaCl_2$ was used to extract the exchangeable fraction (e.g., isovalent Ca^{2+} exchange with Ba^{2+} from clay surfaces). Heavy metals can potentially release via dissolution and re-adsorb to exchangeable sites in response to rapid changes in ambient ionic strength, resulting in re-partitioning among mineral fractions. Step (2) is thus designed immediately after step (1) to minimize potential re-distribution of ions between soluble and exchangeable fractions. Ions associated with these two fractions are readily mobile, hence they are referred to as "labile fraction" in this study.

After removal of the labile fraction, (3) 12 mL 4M acetic acid was used to extract carbonates and iron oxide fractions. High concentrations of acetic acid rapidly decrease the pH value, which enables the desorption of ions from mineral surfaces and potentially causes re-partition. This problem is largely addressed by removing exchangeable ions following step (2), after which the remaining amounts of adsorbed ions are trivial.

(4) 30% hydrogen peroxide, adjusted to pH ~1.5 with HNO_3 at 80 °C, was used to extract the oxidizable fraction; the digestion fluid was continuously added in ~1 ml aliquots

until the dark colored particles were mostly dissolved and the reaction was close to completion with reduced effervescence. Redox reactions mainly happen for iron oxides, organic compounds and sulfides. Since most of the iron oxides and carbonates are removed from step (3), this step mainly extracts organic compounds and sulfides.

(5) 12 mL 0.2M hydroxylamine hydrochloride in 25% acetic acid was then used to extract reducible species (e.g., oxides formed in step (4)). Until this step, the fractions that are easy to dissolve or react with solvents are mostly digested, adsorbed ions are released.

To completely digest silicate minerals, (6a) multiple 12 mL mixtures of hydrofluoric acid (HF) with 0.1N HNO_3 in increasing HF:HNO_3 ratios of 1:9, 1:3, 1:1, 2:1, respectively, were used to complex Si in silicate minerals. Ions complexed with silicate or captured within silicate tetrahedra layers are released after the sequence of reactions. These released ions may immediately adsorb onto other silicate sites or form fluorides. Step (6b) is designed to re-dissolve these newly formed fluorides using 12 mL saturated $AlCl_3$ in 0.1N HNO_3 at 95 °C for 2 h.

In the final steps, insoluble sulfate minerals in the refractory residue are completely dissolved following the Currie-Debye method [44]. Briefly, (7) residue was boiled in 12 mL 1M Na_2CO_3 for 15 h to replace insoluble sulfates with carbonates, i.e. convert barite to barium carbonate, and then harvest the solid and liquid separately, the solid was dissolved with HCl to obtain cations in the sulfate fraction. Additional experiments confirmed the complete dissolution of insoluble sulfates [34].

After the previous 7 steps, the residual was almost negligible (invisible to the naked eyes). To confirm complete digestion of solid samples, (8) reverse aqua regia (HNO_3 : HCl : HF = 1:3:1) was used to dissolve all refractory phases. All extraction steps were

performed at room temperature for 15 hours. The reaction vials were agitated unless otherwise specified. It is possible that small proportions of ions were re-distributed among the eight fractions of sequential extraction steps, but it is likely that the amounts were negligible compared to the values measured after each fraction.

After each of the sequential extraction steps, the liquid was passed through a 0.45 μm membrane, and the solid was rinsed three times with deionized (DI) water. The DI water rinses were combined with the liquid to yield an extractant for that step. The extractants were then acidified to 5% HNO_3 prior to chemical analysis, in order to prevent sulfate precipitation. The solid that remained after the extraction was used for the next digestion step [34,39].

Although filtration can result in loss of sample solids, it is necessary in order to prevent contamination of extractions from particulate solids [34,39,43]. In order to verify the mass recovery of the sequential extraction procedure, we conducted bulk digestions for both RWS and WTS solids. The bulk digestion used a sequence of reagents without separation of solid and liquid fractions in the intermediate steps, therefore mass loss during sample transfer was eliminated. The detailed procedure of the bulk digestion is presented in Supplementary Information. Through bulk digestion, we found that the sequential extraction procedure yielded over 80% of the total elemental mass of that by the bulk digestion. The results are presented without correction for yield.

2.3 Sample characterizations

All samples generated by the sequential extraction were analyzed in the Earth Sciences Department, Dartmouth College, Hanover, NH. The extractants and wastewaters were analyzed for major elements using an ICP-OES (Thermo Iris Intrepid II). Calibration

standards were prepared using NIST-traceable sources provided by Inorganic Ventures (Christiansburg, VA USA). The detection limit of ICP-OES is 0.05 ppm for the cations examined in this study. All samples were run as dilute solutions of HNO_3 with on-line addition of appropriate internal standards (uncertainty introduced by dilution is equal to or less than 0.5 %).

This study measured Ra-226 using HPGe gamma spectrometers (Canberra BEGE3830) for both the liquid extractants and solid samples. Instrumental analysis followed the methods described in Landis *et al*. (2012) [45], with instrument calibration performed using CanMET U-ore BL5 and Th-ore OKA2 in geometries identical to samples. Bulk RWS and WTS solids were measured in 10 cm^3 petri dishes, and self-attenuation was corrected for all gamma energies using a multi-nuclide point source. Detection limit for the gamma spectrometer is 0.2 Bq. For solid powder samples, aliquots of 50 mg of ore powder were mounted by filtration onto 47 mm filter papers for measurements [45]. For liquid extractants, Ra was pre-concentrated as radio-barite prior to mounting on 47 mm quartz fiber filters. We first added a desired amount of 1 M $BaCl_2$, such that the total Ba in solution would produce 50 mg $BaSO_4$. Then excess concentrated H_2SO_4 was added to precipitate Ba and Ra as radio-barite. Calibration for filter geometry was established using U- and Th-ores BL5 and OKA from CanMET mounted identically to samples; standard deviation of replicates (<1%) is included in expanded uncertainties. Ra calibration was confirmed with a NIST-traceable Ra-226 standard obtained from Eckert and Ziegler and prepared by sulfate precipitation as samples. Agreement between U-ore and a NIST-traceable Ra-226 standard was 99.1% ± 2.8% (2-sigma standard error) (see detailed description in Supplementary Information). Sample yields for the precipitation

procedure averaged 92.6% ± 3.1% of the total Ra-226. Each sample was counted for 24 hours. The Ra-226 activity was measured directly at 186.2 keV (Ra-226) and indirectly using the equilibrated (>30 days) Rn daughters at 295.2 keV (Pb-214), 351.9 keV (Pb-214), and 609.6 keV (Bi-214). Interference on the 186 keV emission from U-235 was monitored and was found to be negligible; further studies (not shown here) also indicated no precipitation of U with barite during sample pre-concentration. Radon leakage was measured in Ra-226 radio-barite standards to be <5%. As there was no measurable difference between direct and indirect Ra methods, we thus reported activities as a variance-weighted average of four emission lines. Although Ra-228 was also present in HVHF waste samples, we only show Ra-226 due to the low activity and high analytical uncertainties of Ra-228 measurement compared to Ra-226.

Electron micrographs of the solids were acquired using a Hitachi tabletop TM3000 scanning electron microscope with energy dispersive X-ray spectroscopy (SEM/EDS); the distribution of Ba and Sr was mapped to help identify the mineral phases. The mineral compositions of the solids were characterized using a Bruker D8-Focus X-ray diffractometer (XRD) and these results are presented in the Supplementary Information.

3. RESULTS AND DISCUSSION

This research characterized the mineral partitioning of Ra, Sr, and Ba in the suspended solids contained in produced water generated following HVHF (RWS). Likewise, the mineral partitioning of Ra, Sr, and Ba in solids produced by mixing the liquid portion of flowback water and AMD (WTS) assess the effectiveness of Ra removal by Ra-Ba-SO_4 co-precipitation. Factors (concentrations of Ba, Sr, Ca, SO_4^{2-}) affecting the

efficiency of Ra removal, the possible mechanisms responsible for this efficiency, and long-term sequestration are also discussed.

3.1 Radium, barium, and strontium partitioning in raw waste solid (RWS)

In this study, we refer to elements that were readily released from soluble and exchangeable solid fractions into natural environments as labile fractions. The sequential extraction of RWS showed high Na recovery (Figure 1A) and more than 30% of the total Ba, Sr and Ra-226 (Figure 1B) released from the soluble fraction. Approximately 8-12% of total Ba, Sr, and Ra-226 were extracted from the exchangeable fraction, indicating that they were present in loosely bound mineral positions (e.g., exchangeable sites on organic compounds, clays, oxides) [31,46]. Combined, these two labile fractionations account for more than 50% of total Ra-226 in solids, which is up to 200 times higher than that reported by Zhang *et al*. (2015) for aged waste sludge [33]. The difference in labile Ra-226 suggests that aging waste sludge in impoundments may significantly change Ra-226 distribution among mineral fractions. In comparison with the Marcellus Shale cuttings [39], more than three times greater Ba, Sr, and Ra-226 were extracted from RWS as labile fractions, indicating these elements must have repartitioned in the suspended solids during hydraulic fracturing processes.

Other fractions that contained Ba, Sr and Ra-226 include carbonates/iron oxides, organic compounds, silicates, and sulfate fractions (Figure 1B). The operationally defined fractions of calcium carbonates and iron oxides hosted more than 10% of Ba, Sr and Ra-226. The silicate fraction contained approximately 20% of Ba and Ra-226. Very small percentages (<5%) of Ba, Sr and Ra-226 were found in the sulfate fraction. The proportion of Ba, Sr and Ra-226 in the residual fraction was negligible. These results are very different

from those reported by Zhang *et al*. (2015) for aged waste sludge where residuals (inferred as insoluble sulfate) hosted 50% - 99% of the total Ra-226.

Potential processes that may result in such differences of Ra-226 distribution among fractions include adsorption-desorption, crystallization, dissolution, and precipitation. Under static conditions like in a centralized wastewater impoundment for a long time, slightly oversaturated iron and manganese oxides will undergo slow precipitation and maturation, which provides great surface areas for Ra-226 sorption and reduce labile Ra-226 [27,47]. Slow dissolution and recrystallization of Ra-containing minerals (e.g. amorphous iron and manganese oxides, see Supplementary Information) will result in desorption of Ra-226 from surfaces [39,43,48,49], which transiently increase labile Ra-226 in water; however, this process is usually followed by re-partition into more stable mineral phases (e.g. sulfates and carbonates) [39,43,47,50]. When barite and celestite become oversaturated due to mixing with incompatible fluids (e.g. fluids contain SO_4^{2-}), Ra-226 easily co-precipitates with these sulfates [8,36,40,50]. Aging of the wastewater often provides extended reaction time and reduced advection, which will enhance adsorption of Ra-226 onto existing surfaces of minerals (e.g. clays and oxides) [20,50]. As a result, the amount of labile Ra-226 will significantly decrease for aged waste sludge, and Ra-226 will be re-distributed into more immobile mineral phases.

It is important to note that more than 50% of the Ra-226 found in the soluble and exchangeable fractions can be released either by dissolution of soluble salts or by cation exchange with the fluids in contact with the solid waste. Therefore, the removal and/or immobilization of Ba and Ra in RWS are crucial prior to waste disposal. Indeed, most of the mobile Ba and Ra-226 extracted from the solid can be co-precipitated with SO_4^{2-} to

form $(Ba,Ra)SO_4$ [24,38,40] in the same manner that waste treatment facilities treat the radioactive wastewater.

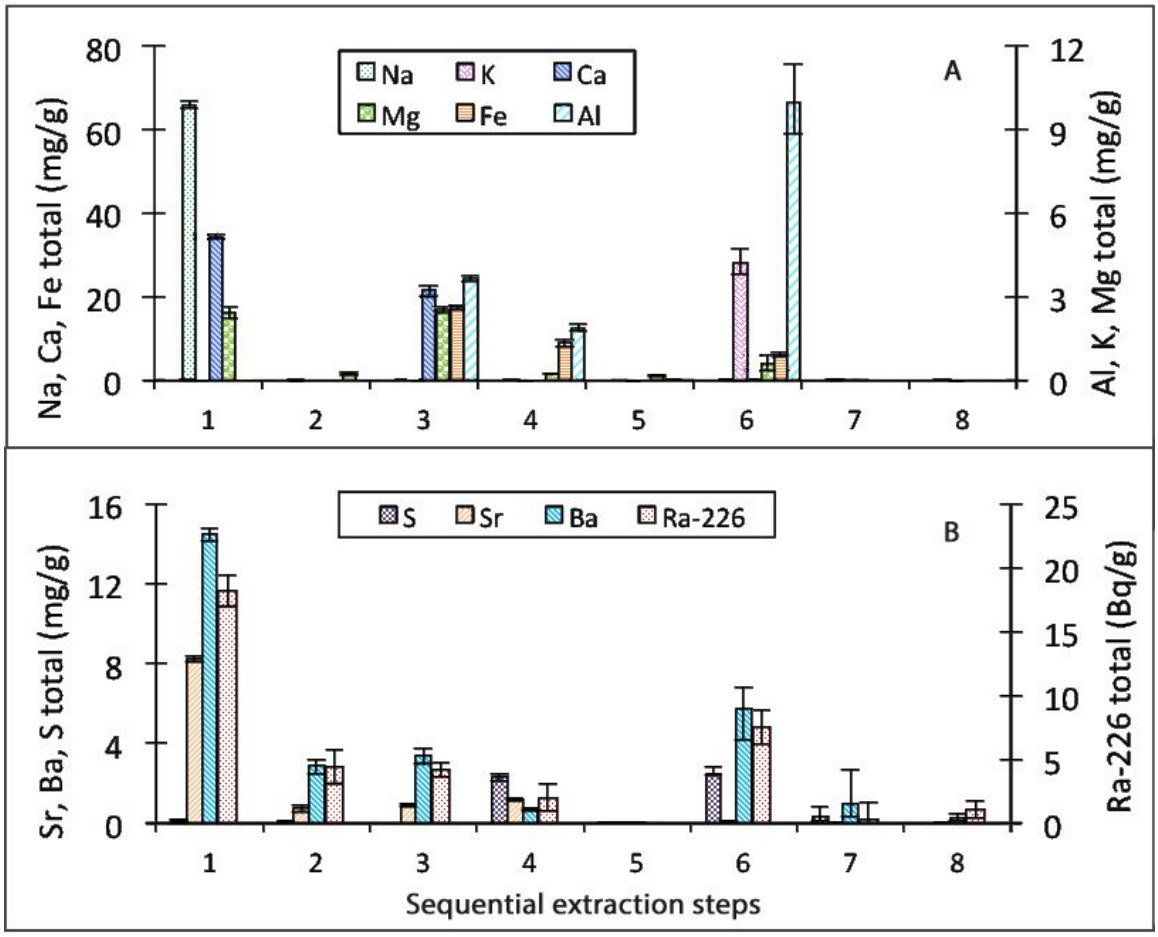

Figure 1. Mean values of (A) major cations and (B) S, Sr, Ba and Ra-226 released in each step of the sequential extraction of raw waste solid expressed in mg/g (or Bq/g for Ra-226). The numbers of sequential extraction steps represent: 1 – soluble fraction, 2 – exchangeable fraction, 3 – carbonate minerals or iron oxides fraction, 4 – organic compounds fraction, 5 – reducible fraction, 6 – silicate fraction, 7 – sulfate fraction, and 8 – residual fraction. Error bars describe the highest and lowest values measured for two parallel experiments.

3.2 Waste treatment solids (WTS) and Ra removal

3.2.1 Elemental composition in WTS

The major cations extracted from the six WTS by the sequential extraction procedure included Na^{+}, Ca^{2+}, Fe^{3+}, Sr^{2+} and Ba^{2+}. The total Ra-226 released from each of the extraction steps 1-6 is below detection limit and therefore not shown. Most of the Na^{+} and Ca^{2+} were present in the soluble fraction; Fe^{3+} appeared mainly in the iron oxides and oxidizable fractions (Figure S4). Figure 2 shows the Ba and Sr contents extracted from the WTS. The elemental compositions released by each extraction step varied among the six WTS due to different compositions of the source liquids and mixing ratios of flowback water to AMD (Tables 1 & 2). After the 6th step (after silicate fraction), 15% to 77% of the total solid weight still remained undissolved, here termed residuals. The residuals contained up to 94% of Ba and over 50% of Sr. These solids were pale-grey in color, and contained primarily sulfate minerals as described below.

Table 1. Mixing ratios of flowback water and AMD and solid yield after treatment

Treatment	Combination	Flowback (mL)	AMD (mL)	Solid dry wt (g)	Wt yield (g/L)	Total Ra-226 in solids* (Bq)	Ra-226 (Bq/g)
1	Flowback I + AMD I	1800	16070	16.0	0.90	700 ± 20	44 ± 1
2	Flowback I + AMD II	7000	10708	79.9	4.51	3120 ± 90	39 ± 1
3	Flowback I + AMD III	1600	16497	13.0	0.72	620 ± 20	47 ± 1
4	Flowback II + AMD I	9600	7603	52.8	3.07	3400 ± 90	64 ± 2
5	Flowback II + AMD II	3200	13707	19.9	1.18	1880 ± 40	95 ± 2
6	Flowback II + AMD III	9000	8780	35.3	1.99	3650 ± 80	103 ± 2

* Calculated from multiplying dry solid weight (g) with concentrations of Ra-226 (Bq/g).

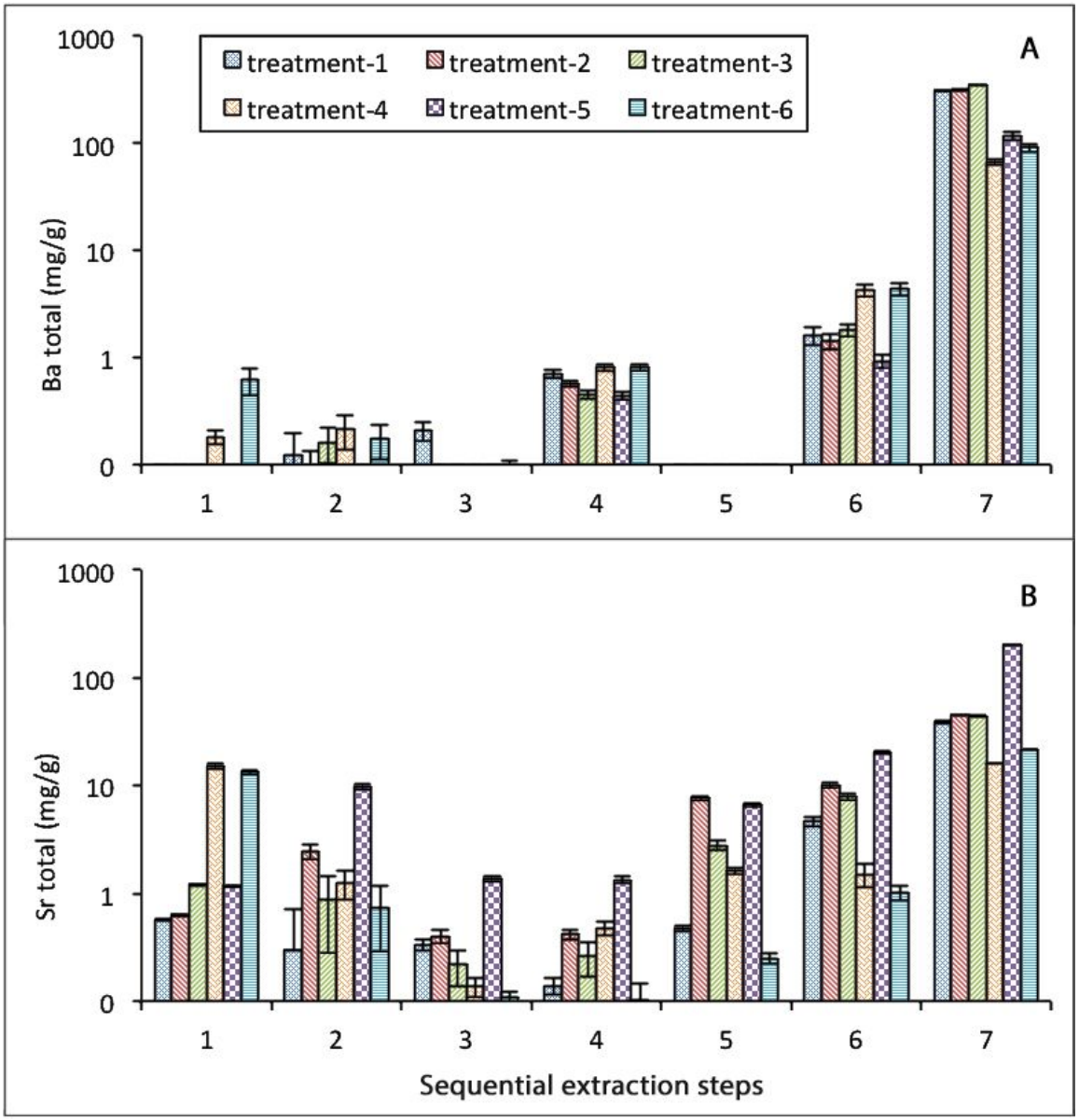

Figure 2. The amount of Ba (A) and Sr (B) released in each step of sequential extraction for six WTS's expressed in mg/g. Error bars describe the highest and lowest values measured for two parallel experiments.

The residual solids after sequential extraction Step 6 were examined for mineralogical compositions using XRD and for particle morphology and elemental compositions using SEM/EDS. XRD results indicated that the residual solids from all treatments (WTS 1 to WTS 6) are barite-celestite mixtures. It is possible that amorphous

solids may not be detected by XRD but serve as important sinks for Ra-226, however, previous rigorous extraction steps have removed most amorphous phases (e.g. iron oxides are dissolved via Step 3, silicates are digested via Step 6), resulting in minimal influence of amorphous phases on Ra-226 distribution. WTS 1-3 was produced using flowback water with a Sr/Ba ratio of 0.68 whereas the ratio in WTS 4-6 was 7.18 (Table 2). We display SEM results of WTS 1 and WTS 4 as representatives for solids formed in treatments of these two Sr/Ba ratios (Figure 3). Before sequential extraction, precipitates consisted of a dark color matrix (and were predominantly composed of Na, Ca, Fe, and Cl) mixed with lighter colored grains (mainly contained Ba, Sr and S) in the electron back-scattered images (Figures 3A and 3D); after sequential extraction Step 6, only light-colored particles remained undissolved. The undissolved solids contained predominately Ba with occurrences of minor Sr as shown in the false colored elemental map (Figures 3C and 3F). When formed in fluids with low Sr/Ba ratios, the precipitates exhibited rounded platy or flaky shapes (Figures 3B & 3C). In contrast, the crystals exhibited hexagonal shapes with clearly defined crystal edges and characteristic orthorhombic habit at higher Sr/Ba ratios (Figures 3E & 3F). This is because the required step energy is lowest when barite crystals grow along [120] crystallographic directions [51], resulting in rhombic crystals as shown in Figure 3B; whereas celestite preferably grows along [010] and [100] directions, forming elongated hexagonal crystals [51,52]. Low Sr/Ba ratios only favor barite precipitation and therefore rhombic crystals, but high Sr/Ba ratios will likely form a mixture of barite and celestite, which forms hexagonal crystals. Except for Sr and Ba, other major elements in undissolved solids are S and O, confirming these particles are sulfate species. In what follows, we refer to the residuals after sequential extraction Step 6 as the sulfate fractions.

Table 2. Chemical composition in liquid mixture of flowback water and AMD prior to precipitation (Panel A) and after precipitation and removal of solids (Panel B).

Treatment	Ba (mM)	Sr (mM)	Ca (mM)	SO_4 (mM)	Ra-226 in liquid (Bq/L)	Ba:Sr:SO_4
Panel A - AMD + flowback before treatment						
1	3.37	2.28	24.42	5.76	42 ± 1	1 : 0.68 : 1.71
2	13.24	8.95	86.01	24.40	179 ± 6	1 : 0.68 : 1.84
3	2.96	2.00	20.44	4.25	34 ± 1	1 : 0.68 : 1.44
4	2.97	21.17	216.65	2.83	203 ± 8	1 : 7.18 : 0.95
5	1.01	7.18	78.96	32.71	112 ± 4	1 : 7.18 : 32.52
6	2.69	19.21	196.08	2.30	211 ± 7	1 : 7.18 : 0.86
Panel B - AMD + flowback after treatment & precipitated solids removed						
1	-	1.76	23.88	1.01	-	0 : 1 : 0.51
2	-	3.71	74.24	4.77	-	0 : 1 : 1.28
3	-	1.60	19.84	1.10	-	0 : 1 : 0.69
4	0.57	20.84	189.83	-	-	1 : 37.07 : 0
5	-	1.20	77.90	18.51	-	0 : 1 : 15.32
6	0.66	18.67	178.00	-	-	1 : 28.33 : 0

- : Chemicals below detection limit.

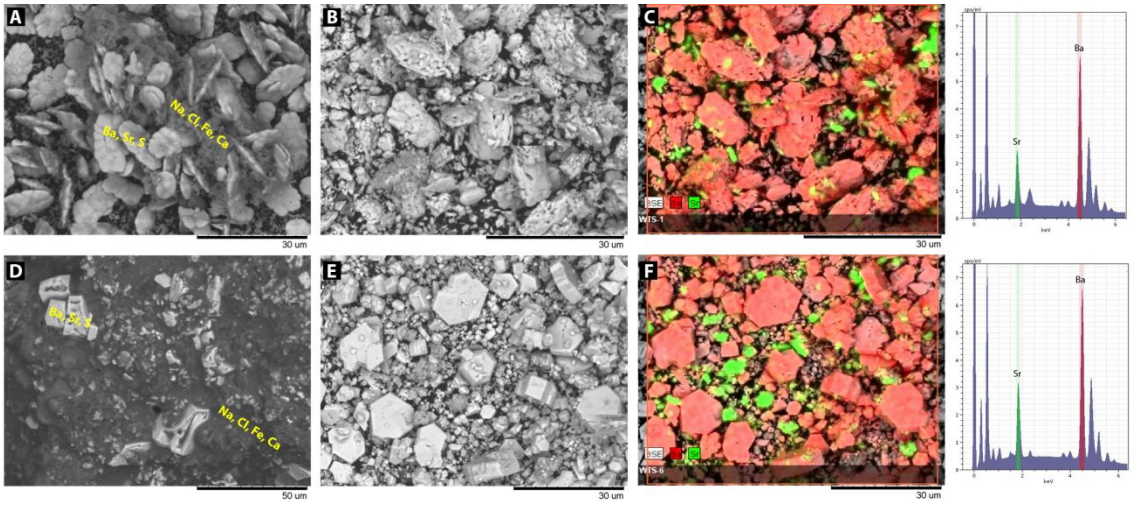

Figure 3. SEM images of representative waste treatment solids: (A) original WTS 1 before sequential extraction procedure, (B) residuals of WTS 1 after sequential extraction Step 6, (C) false color of (B) demonstrating element Ba (red color) and Sr (green color); (D) original WTS 4 before sequential extraction procedure, (E) residuals of WTS 4 after sequential extraction step 6, and (F) false color of (E) demonstrating element Ba (red color) and Sr (green color).

The mass percentages of residual sulfate fraction relative to total precipitated solid in WTS 1-3 and WTS 5 were between 58% and 77%; in contrast, the percentages in WTS 4 and WTS 6 were less than 20%. The higher residual sulfate mass percentage in WTS 1-3 and WTS 5 is likely due to their higher SO_4^{2-} to Ba ratios in the original mixture solution compared with WTS 4 and WTS 6 (Table 2). Note that even though WTS 5 has the same flowback water type as WTS 4 and WTS 6, the WTS 5 used a much larger volume of AMD, thus a much higher SO_4^{2-} concentration to initiate precipitation, the residual sulfate mass yield was also much higher.

The ratios of Ba^{2+}:Sr^{2+}:SO_4^{2-} in mixture solutions dictated the sulfate mineral compositions in precipitated solids, which can be in part demonstrated by thermodynamic calculations. The solubility constants (K_{sp}) of barite and celestite are $10^{-9.97}$ and $10^{-6.63}$, respectively [53,54]. According to Table 3, activity product of $[Ba^{2+}][SO_4^{2-}]$ and $[Sr^{2+}][SO_4^{2-}]$ values are both greater than their respective K_{sp} values in all initial mixture solutions. The saturation indices of barite and celestite in the liquid mixtures (Table 3) were calculated using PHREEQC [55] with Pitzer method [56] (description and detailed inputs are given in Supplementary Information). All solutions were oversaturated with respect to barite and celestite, which is consistent with presence of both minerals in sulfate fractions of all six WTS. However, PHREEQC did not predict celestite precipitation in WTS 4 and 6 (Table 3), despite the significant amounts of Sr that were measured in the sulfate fractions of WTS 4 and 6 [57]. The presence of Sr in the sulfate fractions of WTS 4 and 6 indicated that: 1) contrary to theoretical PHREEQC calculations, independent celestite can precipitate; or 2) Sr was incorporated in barite crystal structure, forming a barite-celestite solid-solution; or 3) a combination of both 1) and 2).

Table 3. Theoretical calculations of solid composition and partition coefficients for Ra in wastewater treatment solids.

Treatment	SI - barite	barite (g)	SI - celestite	celestite (g)	K_d (Ra in barite)*	K_d (Ra in celestite)*
1	3.91	14.17	0.44	0.74	1.75	265.93
2	4.58	57.06	1.14	20.60	3.72	609.20
3	3.9	12.58	0.43	1.08	1.69	254.54
4	2.82	12.21	0.37	0.00	11.29	1697.31
5	3.64	4.10	1.24	21.55	3.16	523.31
6	2.83	11.99	0.38	0.00	9.61	1461.37

* K_d value is calculated following the equations developed by Zhu et al. (2004) [24,54]

For the barite-celestite solid-solution system, past research has shown inconsistent miscibility gaps between the two minerals. Thermodynamic calculations by Prieto *et al.* (2000) demonstrated that the miscibility gap between the two minerals was from 2.1 to 97.9 mole% $SrSO_4$ at 25 °C [58,59], suggesting that, in general, $BaSO_4$ and $SrSO_4$ form relatively pure crystals with a limited capacity for solid-solutions. Whereas, more recent studies showed that barite and celestite are completely miscible at room temperature [60,61]. In our WTS samples, the molar percentages of Sr in the total sulfate fractions varied from 17% to 73%. From SEM/EDS analysis, Ba-rich and Sr-rich sulfate minerals occurred in independent particles (Figure 3). This suggests that relatively pure celestite formed in all WTS samples and that significant miscibility gaps likely exist between barite and celestite in these solids.

3.2.2 Removal of Ra-226

For all WTS's, more than 80% (80-97%) of the Ra-226 was found in the sulfate fraction (Table 4), with negligible amounts in other fractions. This result agreed with previous studies that the treatment of HVHF wastewater through mixing with SO_4^{2-}-rich AMD is effective in removing most of the labile Ra-226 by forming insoluble sulfates [8]. However, the Ra-226 concentrations (or specific activities) in the sulfate fractions are not

constant but varied among different WTS. For WTS 4 and 6, the specific Ra-226 activity in the sulfate fractions are greater than 350 Bq/g, while WTS 1-3 had activity less than 60 Bq/g, with WTS 5 having an intermediate value of 155 Bq/g. This pattern indicated that more Ra-226 was incorporated into the same unit mass of sulfate minerals in WTS 4 and 6 than WTS 1-3 and WTS 5. The result is suggestive of the possibility to concentrate a large amount of Ra-226 into a small quantity of sulfate mineral.

Table 4. Ra-226 in sulfate fraction of waste treatment solid.

Treatment #	Ra-226 original (Bq)	Ra-226 in barite residual (Bq)	Ra-226 yield %	Original mass (g)	Mass residual (g)	Mass yield %
1	95 ± 3	77 ± 4	80.9%	2.15	1.44	67.0%
2	79 ± 3	69 ± 3	87.1%	2.03	1.42	70.1%
3	96 ± 3	85 ± 5	89.2%	2.02	1.55	77.0%
4	131 ± 5	107 ± 6	81.3%	2.04	0.29	14.2%
5	189 ± 6	184 ± 9	97.1%	2.05	1.18	57.6%
6	209 ± 7	171 ± 9	82.3%	2.02	0.35	17.6%

Solution chemistry likely affects Ra-226 co-precipitation through variations in SO_4^{2-}, Ba^{2+}, Sr^{2+} and Ca^{2+} ion concentrations. The Sr/Ba ratio may be the most important factor; it was lower in solution mixtures of WTS 1-3 (0.68) than WTS 4-6 (7.18) by a factor of 10. Strontium and barium are chemically similar and are thus able to co-precipitate, a higher Sr/Ba ratio in solution may lead to the formation of more Sr-enriched sulfate precipitates [8,24,38,62]. Preliminary experimental results on Ra-226 co-precipitation at conditions with varied Sr/Ba ratios and background cations (not shown in this work) supported this mechanism. This phenomenon may also be examined by future researchers. Thermodynamic models also indicate that an increase in Sr/Ba ratio would help incorporating Ra^{2+} in the solid phase [60,61]. A second difference between WTS 1-3 and WTS 4-6 mixtures is the Ca/Ba ratio; the latter is also higher than the former by a factor of 10. Calcium is the second most abundant cation in wastewater produced from HVHF

[10,11,14,16,63] and can potentially compete with Sr and Ba for SO_4^{2-} to form gypsum ($CaSO_4$) [64]. The effect of SO_4^{2-} concentration can be identified by comparing WTS 4 with WTS 5 and 6. Although all three treatments started with the same Sr/Ba and Ca/Ba ratios, the mixture solution of WTS 5 had a significantly higher SO_4^{2-} concentration, and produced a much greater mass of sulfate with a lower specific Ra-226 activity.

The effect of solution chemistry on Ra-226 removal can be quantified by regression analysis. We found a significant positive correlation between the specific activity of Ra-226 and the Sr/Ba ratio ($p=0.043$, $r^2=0.68$), suggesting that Sr promoted Ra-226 removal via sulfate precipitation. Unfortunately, the Sr/Ba ratio was highly correlated with the Ca/Ba ratio ($p<0.0001$, $r^2=1.0$), so that the independent effect of Ca on Ra-226 removal could not be determined using this data set. When the independent effect of SO_4^{2-} concentration was analyzed through a multiple regression of specific Ra-226 activity against both SO_4^{2-}/Ba and Sr/Ba ratios, the model explained 96% of the total variance ($r^2=0.96$, $p=0.0084$), and both partial regression coefficients were significant (Figure 4A & 4B). Again, the multiple regression showed that Sr/Ba ratio was positively correlated with the specific Ra-226 activity, as in the case of simple linear regression described above. When holding Sr/Ba ratio constant, the specific Ra-226 activity is negatively correlated with SO_4^{2-}/Ba ratio, suggesting that high SO_4^{2-}/Ba ratio may increase total sulfate produced by co-precipitation, and thus Ra activity per unit mass of sulfate decreases. This explanation particularly applies to the difference between low Ra-226 specific activity in WTS 5 relative to WTS 4 and 6.

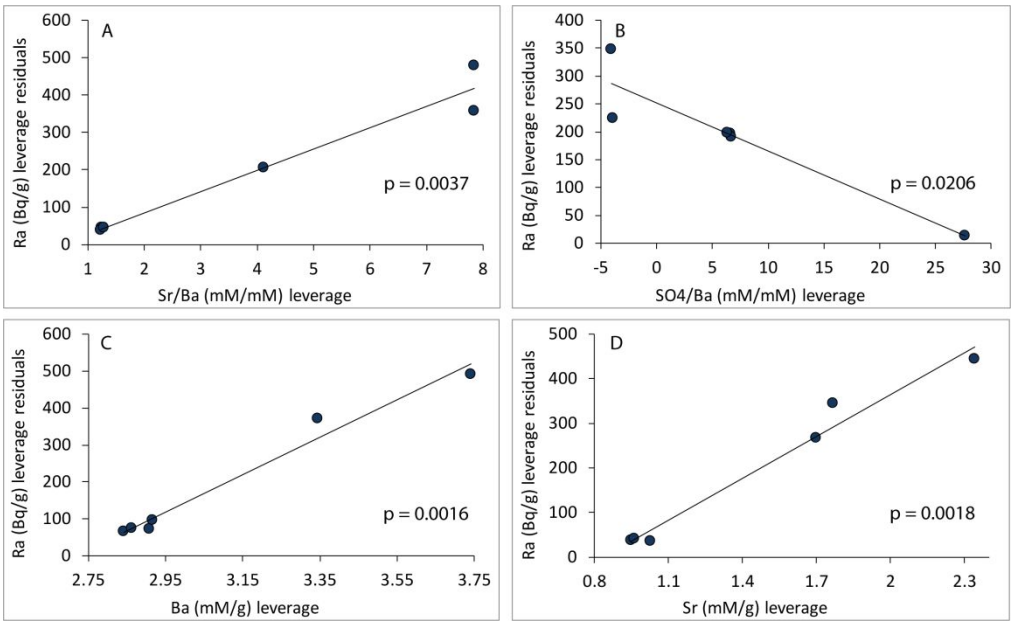

Figure 4. Leverage plots for multiple regressions of specific Ra-226 (Bq/g) in sulfate residual versus (A) Sr/Ba molar ratio and (B) SO_4/Ba molar ratio in the **mixture solution** (for the overall regression, r^2 value is 0.96; p = 0.0084); and leverage plots for multiple regression of specific Ra-226 (Bq/g) versus (C) Ba (mM/g) and (D) Sr (mM/g) concentrations in **sulfate residual** (for the overall regression, r^2 value is 0.98; p = 0.0037).

The effects of Sr and Ba component in the residual sulfate fraction on Ra-226 removal were also demonstrated by regression analysis. The multiple regression of specific Ra-226 activity against both Ba and Sr concentrations in the sulfate fraction explained 98% of the total variance of the Ra-226 specific activity (r^2=0.98, p=0.0037), with both partial regression coefficients significant (Figures 4C & 4D). Interestingly, the partial correlation of Ra-226 with Ba and Sr are both positive with each explaining about half of the variance. This result indicates that when holding Ba constant, Ra-226 increases with increasing Sr in the solid. The same statement applies to Ba when Sr is held constant. The concentration of Ra-226 is increased when either Ba or Sr is increased in sulfate precipitate.

3.2.3 Mechanisms in Ba-Sr-Ra co-precipitation

Previous studies have suggested that Ra is easily incorporated into barite and/or celestite [24,41]. However, the efficiency of Ra removal as a function of Ba and Sr concentrations is inconsistent among studies [38,41,65]. Ceccarello *et al.* (2004) found that the Ra concentration in the solid precipitated from gel column experiments decreased as Sr/Ba ratio increased from 0 to 1 in the original solution [41], whereas Grandia (2008) concluded that an increasing Sr/Ba ratio from 10 to 10,000 enhanced Ra incorporation in the solid [38,65]. Behavior in the Sr/Ba range from 1 to 10 has not been observed by previous investigations.

Two mechanisms of Ra coprecipitation with sulfate have been proposed. In binary systems of Ra-$BaSO_4$ and Ra-$SrSO_4$, the partition coefficients, K_d, between Ra-containing solid and solution ($K_d = \frac{[RaSO_4]}{[MSO_4]} \cdot \frac{[Ra^{2+}]}{[M^{2+}]}$) has been derived from lattice replacement reactions [24,54]. Theoretical calculations suggest that the partition coefficient for Ra-$SrSO_4$ is one to two orders of magnitude greater than that for Ra-$BaSO_4$ (Table 3), indicating that other things being equal, celestite has a greater potential to incorporate Ra-226 than barite. Based on this mechanism, increasing Sr in the solution, particularly to the level that celestite forms independent precipitation, would favor Ra removal. The second mechanism proposed for the tertiary system of Ba-Sr-Ra, is that the presence of Sr may decrease the potential for Ra removal due to the competition of Sr with Ra to enter $BaSO_4$ structure [24,41]. This mechanism has been used to explain experimental results where total Ra removal from the solution decreased with increasing Sr/Ba ratios from 0-1 [41].

Combining the two mechanisms described above, we suggest that in the tertiary Ba-Sr-Ra system, Ra activity in the precipitated sulfate solid varies nonlinearly as a function of the solution Sr/Ba ratio. The specific Ra activity decreases at low ratios but

increases at high ratios. When $[Sr^{2+}][SO_4^{2+}]$ is below celestite saturation, Sr may enter $BaSO_4$ and compete with Ra, causing a decrease in Ra removal with an increase in Sr/Ba ratio. When Sr concentration is sufficiently high to form independent celestite mineral, the high K_d of Ra in celestite relative to barite favors incorporation of Ra into celestite, resulting in enhanced removal of Ra with increasing Sr/Ba ratio. This would explain the apparent contradictory observation in the effect of Sr/Ba ratio on Ra co-precipitation observed in previous studies [38,41,65].

In our experiments, the specific activity of Ra in sulfate is positively correlated with Sr/Ba ratio of the solution (Figure 4A). We propose that the main mechanism for this observation is the thermodynamic variation of K_d as a function of the sulfate mineral types (barite vs. celestite) and the solution chemistry. First, in our AMD-HVHF solutions, the K_d for celestite (~250-1700) is over 100 fold greater than that for barite (~1.7-11.3) (Table 3). As a result, formation of celestite would significantly promote Ra co-precipitation. Second, solution chemistry also affects K_d values (Table 3). The strongest evidence is the six-fold higher theoretical K_d value for WTS 4 and 6, and therefore higher Ra-226 specific activity in residuals, compared to the four other treatments (WTS 1-3 and WTS 5).

Based on our proposed co-precipitation mechanism in the Ba-Sr-Ra-SO_4 system, the efficiency of Ra removal should depend not only on the Sr/Ba ratio, but also on ion concentrations, particularly sulfate concentrations, which partially determines the formation of celestite. Further study is designed to fully examine the combined influence of the partition coefficient and background solution on Ra co-precipitation. Although past studies have reported high concentrations of Ca^{2+} in wastewater and polluted sites [4,15,24,33,66,67], its influence on Ra removal and the underlying mechanisms is rarely discussed

[38]. In this study, unfortunately, our data do not provide sufficient degrees of freedom to constrain the independent effect of Ca^{2+} on Ra co-precipitation in flowback water. Additional study is required to clarify the effects of Ca^{2+} on Ra removal.

3.4 Environmental implications

Large volumes of oil and gas wastewater are generated each year [1–6]. The solid waste separated from the wastewater contains a mixture of soluble salts, carbonates, oxides, organic compounds, silicates and sulfates (Figure 1) [33] and are currently hauled to landfills for disposal. The majority of the Ra is associated with soluble salts, oxides, carbonates and organic compounds that is released relatively easily to the environment, whereas Ra in silicates and sulfates is more resistant to weathering and remains stable for a longer time period [34]. Our work showed that more than 50% of Ra-226 is associated with soluble salts and/or easily exchangeable with cations in solution. This characterization of waste materials provides insights into potential pathways for Ra release after disposal and helps establish protocols for proper HVHF wastewater disposal [68–70].

Removal of Ra-226 from HVHF wastewater by co-precipitation with Ba^{2+} and SO_4^{2-} has been studied in recent years [8,18,33,40]. Such co-precipitation immobilizes Ra-226 into insoluble barite [71,72], and thus reduces potential releases of Ra-226 to natural waters or landfills. Specifically, mixing HVHF wastewater and AMD to form $(Ba,Ra)SO_4$ offers an effective means of treatment to the two sources in one process [18]. Through sequential extraction of WTS, we found that mixtures of HVHF wastewater and AMD resulted in precipitation of soluble salts, iron oxides, and a large proportion of insoluble sulfates (barite and/or celestite); more than 80% of Ra-226 originally dissolved in solution was incorporated into the sulfates. The Sr/Ba ratios in the flowback water influenced the cation

composition of the precipitated sulfates (Figure 3 & 4), and the efficiency of Ra removal. Under our experimental conditions, higher Sr/Ba ratios of the flowback-AMD mixture solution resulted in higher specific Ra activity in sulfates. These findings support the means of Ra removal from HVHF wastewater using AMD, and provide guidance for specifically adjusting mixing ratios of waste for effective Ra co-precipitation in minimal volume of solid wastes.

4. CONCLUSIONS

This paper examined the distribution of Ra-226 among mineral fractions in wastes associated with HVHF and provided insights to effective long-term Ra removal practice. In raw waste solids generated by HVHF more than 50% of Ra-226 was found to be labile. In contrast with the 14% labile Ra-226 in Marcellus Shale cuttings [39], the Ra-226 in the raw waste solids become much more mobile. Direct disposal of these waste solids may leak Ra-226 to the surrounding environment, thus proper treatment of the labile Ra-226 prior to disposal is important. During treatment of Ra-226 by mixing AMD and HVHF wastewater, solution chemistry controls the efficiency of Ra-226 removal. Co-precipitation as insoluble sulfate minerals (barite or celestite) can effectively remove Ra for long-term. High Sr/Ba ratios favor Ra-226 sequestration into the same mass of sulfate due to much higher K_d effect of celestite. In Ra treatment, raising Sr/Ba ratios and increasing SO_4^{2-} concentrations can be used to increase Ra removal efficiency. To thoroughly understand how Ra removal is influenced by Sr/Ba ratios at a wide range (e.g. from 0.1 to 100), the presence of Ca^{2+} cation, as well as the background salinity, follow-up experiments are expected. In addition, the variation of K_d in different conditions and the role of K_d on Ra co-precipitation also need further study.

ASSOCIATED CONTENT

Supplementary Information

Additional details of the materials and results for sequential extraction are provided. This material is available at http://rsc.li/process-impacts.

CONFLICT OF INTEREST

There are no conflicts to declare.

ACKNOWLEDGEMENTS

The authors would like to thank Bureau of Abandoned Mine Reclamation, PA and a private waste treatment facility for providing valuable waste materials, and Edward Myer from Dartmouth College for providing technical support. The authors also greatly appreciate the constructive comments and suggestions from the editors and three anonymous reviewers. This work was financially supported by Dartmouth College. The authors declare no competing financial interest.

REFERENCES

(1) Balashov, V. N.; Engelder, T.; Gu, X.; Fantle, M. S.; Brantley, S. L. A Model Describing Flowback Chemistry Changes with Time after Marcellus Shale Hydraulic Fracturing. *A.A.P.G. Bulletin* **2015**, *99* (1), 143–154.

(2) Burgos, W. D.; Castillo-Meza, L.; Tasker, T. L.; Geeza, T. J.; Drohan, P. J.; Liu, X.; Landis, J. D.; Blotevogel, J.; McLaughlin, M.; Borch, T.; et al. Watershed-Scale Impacts from Surface Water Disposal of Oil and Gas Wastewater in Western Pennsylvania. *Environ. Sci. Technol.* **2017**, *51* (15), 8851–8860.

(3) Curtis, J. B. Fractured Shale-Gas Systems. *AAPG Bulletin* **2002**, *86* (11), 1921–1938.

(4) Gregory, K. B.; Vidic, R. D.; Dzombak, D. A. Water Management Challenges Associated with the Production of Shale Gas by Hydraulic Fracturing. *Elements* **2011**, *7* (3), 181–186.

(5) Kondash, A.; Vengosh, A. Water Footprint of Hydraulic Fracturing. *Environ. Sci. Technol. Lett.* **2015**, *2* (10), 276–280.
(6) Lutz, B. D.; Lewis, A. N.; Doyle, M. W. Generation, Transport, and Disposal of Wastewater Associated with Marcellus Shale Gas Development. *Water Resources Research* **2013**, *49* (2), 647–656.
(7) Vengosh, A.; Jackson, R. B.; Warner, N.; Darrah, T. H.; Kondash, A. A Critical Review of the Risks to Water Resources from Unconventional Shale Gas Development and Hydraulic Fracturing in the United States. *Environ. Sci. Technol.* **2014**, *48* (15), 8334–8348.
(8) Kondash, A. J.; Warner, N. R.; Lahav, O.; Vengosh, A. Radium and Barium Removal through Blending Hydraulic Fracturing Fluids with Acid Mine Drainage. *Environ. Sci. Technol.* **2014**, *48* (2), 1334–1342.
(9) Rowan, E. L.; Engle, M. A.; Kirby, C. S.; Kraemer, T. F. *Radium Content of Oil- and Gas-Field Produced Waters in the Northern Appalachian Basin (USA): Summary and Discussion of Data*; U.S. Geological Survey, 2011; p 31.
(10) Barbot, E.; Vidic, N. S.; Gregory, K. B.; Vidic, R. D. Spatial and Temporal Correlation of Water Quality Parameters of Produced Waters from Devonian-Age Shale Following Hydraulic Fracturing. *Environ. Sci. Technol.* **2013**, *47* (6), 2562–2569.
(11) Dresel, P. E.; Rose, A. W.; Rendell, E. G.; Secretary, J. Q.; Dunn, C. A.; Secretary, D.; Dresel, P. E.; Rose, A. W. *Chemistry and Origin of Oil and Gas Well Brines in Western Pennsylvania: Pennsylvania Geological Survey*; Open-File Report OFOG10-01.0: 48pp Open-File Report OFOG10-01.0: 48pp; 2010.
(12) Rowan, E. L.; Engle, M. A.; Kraemer, T. F.; Schroeder, K. T.; Hammack, R. W.; Doughten, M. W. Geochemical and Isotopic Evolution of Water Produced from Middle Devonian Marcellus Shale Gas Wells, Appalachian Basin, PennsylvaniaGeochemistry of Produced Water from Marcellus Shale Water, PA. *AAPG Bulletin* **2015**, *99* (2), 181–206.
(13) Ferrer, I.; Thurman, E. M. Chemical Constituents and Analytical Approaches for Hydraulic Fracturing Waters. *Trends in Environmental Analytical Chemistry* **2015**, *5*, 18–25.
(14) Shih, J.-S.; Saiers, J. E.; Anisfeld, S. C.; Chu, Z.; Muehlenbachs, L. A.; Olmstead, S. M. Characterization and Analysis of Liquid Waste from Marcellus Shale Gas Development. *Environ. Sci. Technol.* **2015**, *49* (16), 9557–9565.
(15) Ferrar, K. J.; Michanowicz, D. R.; Christen, C. L.; Mulcahy, N.; Malone, S. L.; Sharma, R. K. Assessment of Effluent Contaminants from Three Facilities Discharging Marcellus Shale Wastewater to Surface Waters in Pennsylvania. *Environ. Sci. Technol.* **2013**, *47* (7), 3472–3481.
(16) Swann, C.; Matthews, J.; Ericksen, R.; Kuszmaul, J. *Evaluations of Radionuclides of Uranium, Thorium, and Radium Associated with Produced Fluids, Precipitates, and Sludges from Oil, Gas, and Oilfield Brine Injection Wells in Mississippi*; University of Mississippi (US), 2004.
(17) Guerra, K. *Oil and Gas Produced Water Management and Beneficial Use in the Western United States*; U.S. Department of the Interior, Bureau of Reclamation, 2011.

(18) He, C.; Zhang, T.; Zheng, X.; Li, Y.; Vidic, R. D. Management of Marcellus Shale Produced Water in Pennsylvania: A Review of Current Strategies and Perspectives. *Energy Technology* **2014**, *2* (12), 968–976.
(19) Warner, N. R.; Christie, C. A.; Jackson, R. B.; Vengosh, A. Impacts of Shale Gas Wastewater Disposal on Water Quality in Western Pennsylvania. *Environ. Sci. Technol.* **2013**, *47* (20), 11849–11857.
(20) Sajih, M.; Bryan, N. D.; Livens, F. R.; Vaughan, D. J.; Descostes, M.; Phrommavanh, V.; Nos, J.; Morris, K. Adsorption of Radium and Barium on Goethite and Ferrihydrite: A Kinetic and Surface Complexation Modelling Study. *Geochimica et Cosmochimica Acta* **2014**, *146*, 150–163.
(21) Missana, T.; Colàs, E.; Grandia, F.; Olmeda, J.; Mingarro, M.; García-Gutiérrez, M.; Munier, I.; Robinet, J.-C.; Grivé, M. Sorption of Radium onto Early Cretaceous Clays (Gault and Plicatules Fm). Implications for a Repository of Low-Level, Long-Lived Radioactive Waste. *Applied Geochemistry* **2017**, *86*, 36–48.
(22) Szabo, Z.; dePaul, V. T.; Fischer, J. M.; Kraemer, T. F.; Jacobsen, E. Occurrence and Geochemistry of Radium in Water from Principal Drinking-Water Aquifer Systems of the United States. *Applied Geochemistry* **2012**, *27* (3), 729–752.
(23) Icenhour, A. S. *Transport of Radioactive Material by Alpha Recoil*; ORNL/TM--2005/22; ORNL (US). Funding organisation: US Department of Energy (United States), 2005.
(24) Zhang, T.; Gregory, K.; Hammack, R. W.; Vidic, R. D. Co-Precipitation of Radium with Barium and Strontium Sulfate and Its Impact on the Fate of Radium during Treatment of Produced Water from Unconventional Gas Extraction. *Environ. Sci. Technol.* **2014**, *48* (8), 4596–4603.
(25) Rosenberg, Y. O.; Metz, V.; Oren, Y.; Volkman, Y.; Ganor, J. Co-Precipitation of Radium in High Ionic Strength Systems: 2. Kinetic and Ionic Strength Effects. *Geochimica et Cosmochimica Acta* **2011**, *75* (19), 5403–5422.
(26) de Dinis, M. L.; Fiúza, A. Simulation of Liberation and Transport of Radium from Uranium Tailings. In *Uranium in the Environment: Mining Impact and Consequences*; Merkel, B. J., Hasche-Berger, A., Eds.; Springer Berlin Heidelberg: Berlin, Heidelberg, 2006; pp 609–618.
(27) IAEA. The Environmental Behaviour of Radium: Revised Edition. **2014**.
(28) Fleischer, R. L. Isotopic Disequilibrium of Uranium: Alpha-Recoil Damage and Preferential Solution Effects. *Science* **1980**, *207* (4434), 979–981.
(29) Tricca, A.; Wasserburg, G. J.; Porcelli, D.; Baskaran, M. The Transport of U- and Th-Series Nuclides in a Sandy Unconfined Aquifer. *Geochimica et Cosmochimica Acta* **2001**, *65* (8), 1187–1210.
(30) Beiser, A. "Chapter 12: Nuclear Transformations". Concepts of Modern Physics; McGraw-Hill, 2003; pp 432–434.
(31) Wang, R. S.; Chau, A. S. Y.; Liu, F.; Cheng, H.; Nar, P.; Chen, X. M.; Wu, Q. Y. Studies on the Adsorption and Migration of Radium in Natural Minerals. *Journal of Radioanalytical and Nuclear Chemistry, Articles* **1993**, *171* (2), 347–364.
(32) Nelson, A. W.; Johns, A. J.; Eitrheim, E. S.; Knight, A. W.; Basile, M.; Bettis, E. A.; Schultz, M. K.; Forbes, T. Z. Partitioning of Naturally-Occurring Radionuclides (NORM) in Marcellus Shale Produced Fluids Influenced by Chemical Matrix. *Environ Sci Process Impacts* **2016**, *18* (4), 456–463.

(33) Zhang, T.; Hammack, R. W.; Vidic, R. D. Fate of Radium in Marcellus Shale Flowback Water Impoundments and Assessment of Associated Health Risks. *Environ. Sci. Technol.* **2015**, *49* (15), 9347–9354.
(34) Renock, D.; Landis, J. D.; Sharma, M. Reductive Weathering of Black Shale and Release of Barium during Hydraulic Fracturing. *Applied Geochemistry* **2016**, *65*, 73–86.
(35) Vengosh, A.; Warner, N.; Jackson, R.; Darrah, T. The Effects of Shale Gas Exploration and Hydraulic Fracturing on the Quality of Water Resources in the United States. *Procedia Earth and Planetary Science* **2013**, *7*, 863–866.
(36) Gordon, L.; Rowley, K. Coprecipitation of Radium with Barium Sulfate. *Anal. Chem.* **1957**, *29* (1), 34–37.
(37) Doerner, H. A.; Hoskins, W. M. CO-PRECIPITATION OF RADIUM AND BARIUM SULFATES1. *J. Am. Chem. Soc.* **1925**, *47* (3), 662–675.
(38) Grandia, F.; Merino, J.; Bruno, J. *Assessment of the Radium-Barium Co-Precipitation and Its Potential Influence on the Solubility of Ra in the near-Field*; Swedish Nuclear Fuel and Waste Management Co., 2008.
(39) Landis, J. D.; Sharma, M.; Renock, D.; Niu, D. Rapid Desorption of Radium Isotopes from Black Shale during Hydraulic Fracturing. 1. Source Phases That Control the Release of Ra from Marcellus Shale. *Chemical Geology* **2018**, *496*, 1–13.
(40) He, C.; Zhang, T.; Vidic, R. D. Co-Treatment of Abandoned Mine Drainage and Marcellus Shale Flowback Water for Use in Hydraulic Fracturing. *Water Res.* **2016**, *104*, 425–431.
(41) Ceccarello, S.; Black, S.; Read, D.; Hodson, M. E. Industrial Radioactive Barite Scale: Suppression of Radium Uptake by Introduction of Competing Ions. *Minerals Engineering* **2004**, *17* (2), 323–330.
(42) Blondes, M. S.; Gans, K. D.; Engle, M. A.; Kharaka, Y. K.; Reidy, M. E.; Saraswathula, V.; Thordsen, J. J.; Rowan, E. L.; Morrissey, E. A. U.S. Geological Survey National Produced Waters Geochemical Database v2.3 (Provisional) https://energy.usgs.gov/EnvironmentalAspects/EnvironmentalAspectsofEnergyProductionandUse/ProducedWaters.aspx#3822349-data (accessed Oct 8, 2018).
(43) Landis, J. D.; Sharma, M.; Renock, D. Rapid Desorption of Radium Isotopes from Black Shale during Hydraulic Fracturing. 2. A Model Reconciling Radium Extraction with Marcellus Wastewater Production. *Chemical Geology* **2018**.
(44) Cohen, A. S.; O'Nions, R. K. Precise Determination of Femtogram Quantities of Radium by Thermal Ionization Mass Spectrometry. *Anal. Chem.* **1991**, *63* (23), 2705–2708.
(45) Landis, J. D.; Renshaw, C. E.; Kaste, J. M. Measurement of 7Be in Soils and Sediments by Gamma Spectroscopy. *Chemical Geology* **2012**, *291*, 175–185.
(46) Tamamura, S.; Takada, T.; Nagao, S.; Yamamoto, M.; Tomita, J.; Fukushi, K. Salinity Dependence of Ra-226 Adsorption on Montmorillonite and Kaolinite. *Journal of Radioanalytical and Nuclear Chemistry* **2014**, *299* (1), 569–575.
(47) Barescut, J. C.; Gariel, J. C.; Péres, J. M.; Bassot, S.; Stammose, D.; Benitah, S. Radium Behaviour during Ferric Oxi-Hydroxides Ageing. *Radioprotection* **2005**, *40* (S1), S277–S283.

(48) Webster, I. T.; Hancock, G. J.; Murray, A. S. Modelling the Effect of Salinity on Radium Desorption from Sediments. *Geochimica et Cosmochimica Acta* **1995**, *59* (12), 2469–2476.

(49) Gonneea, M. E.; Morris, P. J.; Dulaiova, H.; Charette, M. A. New Perspectives on Radium Behavior within a Subterranean Estuary. *Marine Chemistry* **2008**, *109* (3), 250–267.

(50) Martin, P.; Akber, R. A. Radium Isotopes as Indicators of Adsorption–Desorption Interactions and Barite Formation in Groundwater. *Journal of Environmental Radioactivity* **1999**, *46* (3), 271–286.

(51) Becker, U.; Biswas, S.; Kendall, T.; Risthaus, P.; Putnis, C. V.; Pina, C. M. Interactions between Mineral Surfaces and Dissolved Species: From Monovalent Ions to Complex Organic Molecules. *Am J Sci* **2005**, *305* (6–8), 791–825.

(52) Wilcock, J. R.; Perry, C. C.; Williams, R. J. P.; Brook, A. J. Biological Minerals Formed from Strontium and Barium Sulphates. II. Crystallography and Control of Mineral Morphology in Desmids. *Proc. R. Soc. Lond. B* **1989**, *238* (1292), 203–221.

(53) Helgeson, H. C.; Delany, J. M.; Nesbitt, H. W.; Bird, D. K. Summary and Critique of the Thermodynamic Properties of Rock-Forming Minerals /. *American Journal of Science* **1978**, 278-A(3).

(54) Zhu, C. Coprecipitation in the Barite Isostructural Family: 1. Binary Mixing Properties 11Associate Editor: J. D. Rimstidt. *Geochimica et Cosmochimica Acta* **2004**, *68* (16), 3327–3337.

(55) Parkhurst, D. L. User's Guid to PHREEQC: A Computer Program for Speciation, Reaction-Path, Advective-Transport, and Inverse Geochemical Calculations. *Lakewood, Colo.: Denver, CO :U.S. Dept. of the Interior, U.S. Geological Survey; Earth Science Information Center, Open-File Reports Section [distributor]* **1995**.

(56) Pitzer, K. S. Thermodynamics of Electrolytes. I. Theoretical Basis and General Equations. *J. Phys. Chem.* **1973**, *77* (2), 268–277.

(57) Zermeno-Motante, M. I.; Nieto-Delgado, C.; Cannon, F. S.; Cash, C. C.; Wunz, C. C. Chemical Modeling for Precipitation from Hypersaline Hydrofracturing Brines. *Water Res.* **2016**, *103*, 233–244.

(58) Prieto, M.; Fernández-González, A.; Becker, U.; Putnis, A. Computing Lippmann Diagrams from Direct Calculation of Mixing Properties of Solid Solutions: Application to the Barite-Celestite System. *Aquatic Geochemistry* **2000**, *6* (2), 133–146.

(59) Becker, U.; Fernández-González, A.; Prieto, M.; Harrison, R.; Putnis, A. Direct Calculation of Thermodynamic Properties of the Barite/Celestite Solid Solution from Molecular Principles. *Phys Chem Min* **2000**, *27* (4), 291–300.

(60) Vinograd, V. L.; Kulik, D. A.; Brandt, F.; Klinkenberg, M.; Weber, J.; Winkler, B.; Bosbach, D. Thermodynamics of the Solid Solution - Aqueous Solution System (Ba,Sr,Ra)SO4 + H2O: I. The Effect of Strontium Content on Radium Uptake by Barite. *Applied Geochemistry* **2018**, *89*, 59–74.

(61) Heberling, F.; Schild, D.; Degering, D.; Schäfer, T. How Well Suited Are Current Thermodynamic Models to Predict or Interpret the Composition of (Ba,Sr)SO4 Solid-Solutions in Geothermal Scalings? *Geotherm Energy* **2017**, *5* (1), 9.

(62) Abidi, R.; Slim-Shimi, N.; Marignac, C.; Hatira, N.; Gasquet, D.; Renac, C.; Soumarin, A.; Gleeson, S. The Origin of Sulfate Mineralization and the Nature of the BaSO4–SrSO4 Solid-Solution Series in the Ain Allega and El Aguiba Ore Deposits, Northern Tunisia. *Ore Geology Reviews* **2012**, *48*, 165–179.

(63) Chapman, E. C.; Capo, R. C.; Stewart, B. W.; Kirby, C. S.; Hammack, R. W.; Schroeder, K. T.; Edenborn, H. M. Geochemical and Strontium Isotope Characterization of Produced Waters from Marcellus Shale Natural Gas Extraction. *Environ. Sci. Technol.* **2012**, *46* (6), 3545–3553.

(64) Averyt, K. B.; Paytan, A. Empirical Partition Coefficients for Sr and Ca in Marine Barite: Implications for Reconstructing Seawater Sr and Ca Concentrations. *Geochemistry, Geophysics, Geosystems* **2003**, *4* (5).

(65) Goldschmidt, B. On Mixed Precipitation of Sulphates of Barium and Strontium. *Comptes Rendus Hebdomadaires Des Seances De L Academie Des Sciences* **1938**, No. 206, 1110–1113.

(66) Dalvi, A. A.; Kumar, S. D.; Reddy, A. V. R. A Site-Specific Study on the Measurement of Sorption Coefficients for Radionuclides. *Int. J. Environ. Sci. Technol.* **2014**, *11* (3), 617–622.

(67) Renou, S.; Givaudan, J. G.; Poulain, S.; Dirassouyan, F.; Moulin, P. Landfill Leachate Treatment: Review and Opportunity. *Journal of Hazardous Materials* **2008**, *150* (3), 468–493.

(68) van der Sloot, H. A.; van Zomeren, A.; Meeussen, J. C. L.; Seignette, P.; Bleijerveld, R. Test Method Selection, Validation against Field Data, and Predictive Modelling for Impact Evaluation of Stabilised Waste Disposal. *Journal of Hazardous Materials* **2007**, *141* (2), 354–369.

(69) van der Sloot, H. A.; Kosson, D. S.; Hjelmar, O. Characteristics, Treatment and Utilization of Residues from Municipal Waste Incineration. *Waste Management* **2001**, *21* (8), 753–765.

(70) van der Sloot, H. A.; Meeussen, J. C. L.; van Zomeren, A.; Kosson, D. S. Developments in the Characterisation of Waste Materials for Environmental Impact Assessment Purposes. *Journal of Geochemical Exploration* **2006**, *88* (1), 72–76.

(71) Blount, C. W. Barite Solubilities and Thermodynamic Quantities up to 300 Degrees C and 1400 Bars. *American Mineralogist* **1977**, *62* (9–10), 942–957.

(72) Risthaus, P.; Bosbach, D.; Becker, U.; Putnis, A. Barite Scale Formation and Dissolution at High Ionic Strength Studied with Atomic Force Microscopy. *Colloids and Surfaces A: Physicochemical and Engineering Aspects* **2001**, *191* (3), 201–214.

Table of Contents Entry

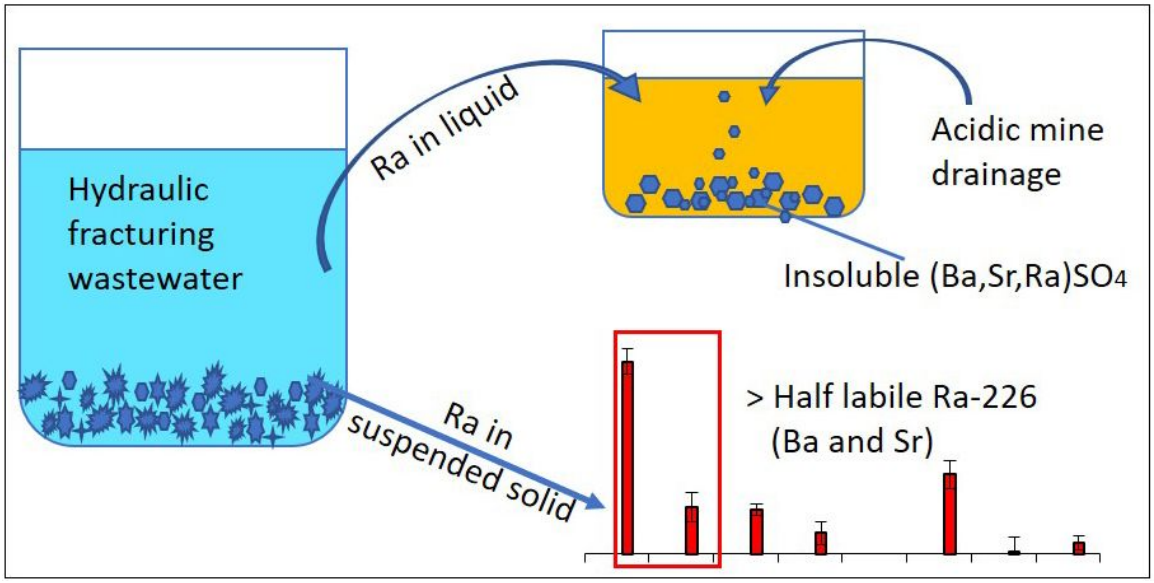

More than half of Ra-226 in waste solid is labile, which can be immobilized by AMD with proper chemistry.